Mon. Not. R. Astron. Soc. **000**, 000–000 (0000) Printed 1 February 2008 (MN LATEX style file v1.4)

Mass constraints from multiphase cooling flow models

Peter A. Thomas
Astronomy Centre, School of Chemistry, Physics and Environmental Science, University of Sussex, Falmer, Brighton BN1 9QH

Accepted —. Received —; in original form —

ABSTRACT
I review the multiphase cooling flow equations that reduce to a relatively simple form for a wide class of self-similar density distributions described by a single parameter, k. It is shown that steady-state cooling flows are *not* consistent with all possible emissivity profiles which can therefore be used as a test of the theory. In combination, they provide strong constraints on the temperature profile and mass distribution within the cooling radius. The model is applied to ROSAT HRI data for 3 Abell clusters. At one extreme ($k \sim 1$) these show evidence for cores in the mass distribution of size 110–140 h_{50}^{-1}kpc and have temperatures which decline towards the flow centre. At the other ($k \mapsto \infty$), the mass density and gas temperature both rise sharply towards the flow centre. The former are more consistent with measured temperatures, which suggests that the density distribution in the intracluster medium contains the minimum possible mixture of low-density components.

Key words: cooling flows — dark matter

1 INTRODUCTION

The multiphase nature of the intracluster medium (ICM) in cooling flows was demonstrated a decade ago when deprojections of X-ray surface-brightness profiles showed that mass cools and is deposited from the flow in a distributed manner, $\dot{M} \propto r$ (e.g. Thomas, Fabian & Nulsen 1987). However, the complexity of the theory and lack of data with high spatial resolution means that the single-phase approximation is still widely adopted. In this paper I show how the use of self-similar density distributions can lead to a relatively simple form for the multiphase cooling flow equations whilst spanning the whole range of expected behaviours in the more general case. In combination with the emissivity profile (for a spherically-symmetric flow), the equations can be solved to yield the gas temperature and mass profiles within the cooling flow.

In Section 2, I introduce the concept of the volume fraction to describe the distribution of density phases in the ICM. The self-similar forms of the volume fraction are determined and shown to span all reasonable behaviours for the more general situation. The steady-state, self-similar form of the cooling flow equations are derived in Section 3 and it is shown how these can be solved in the spherically-symmetric case if the emissivity profile is known. The behaviour of the solutions is examined in detail: not every emissivity profile is consistent with these models. In Section 4, the theory is applied to ROSAT HRI data for three Abell clusters with some success. Finally, the results are summarised and further discussed in Section 5.

2 THE FORM OF THE DENSITY DISTRIBUTION

The theory of multiphase cooling flows was set out by Nulsen (1986). He introduced the concept of the volume fraction, $f(\rho, \mathbf{r}, t)$, such that $f\,\mathrm{d}\rho$ is the fractional volume occupied by phases with densities in the range ρ to $\rho + \mathrm{d}\rho$. It is assumed that the phases comove but are thermally isolated from one another—these can be regarded as empirical facts as otherwise the flow would rapidly evolve to a single-phase state.

Given these assumptions then it is relatively straightforward to derive an equation for the evolution of the volume fraction (see Appendix). Writing

$$f = \frac{(2-\alpha)}{\rho_0} w^{(4-\alpha)/(2-\alpha)} g(w, \mathbf{r}, t), \tag{1}$$

where

$$w = \left(\frac{\rho_0}{\rho}\right)^{2-\alpha} \tag{2}$$

and $\rho = \rho(\mathbf{r}, t)$, then

$$\frac{\dot{g}}{g} + (3-\alpha)\frac{\dot{\rho_0}}{\rho_0} - \frac{2-\alpha}{\gamma}\frac{\dot{P}}{P} + \nabla.\mathbf{u} = 0 \tag{3}$$

where the dot refers to a covariant derivate, following the flow.

In general g is a complicated function of position and time. However, we can look for solutions in which g has a constant functional form, $g = g(w)$. Only the first term

in equation 3 depends upon w. Hence we require that $\dot{g} \equiv \dot{w}\,\mathrm{d}g/\mathrm{d}w \propto g$. There are two kinds of solution:

(i) $g_\infty \propto \exp(-w)$. This is the most extended distribution which is convectively stable (it gives $P \propto \rho_0^\gamma$). It includes phases of arbitrarily low density.

(ii) $g_k \propto (1-w)^{k-1}$, $0 < w < 1$; $k \geq 1$. These solutions possess a minimum density, $\rho \geq \rho_0$. $k = 1$ is the least extended, consisting solely of the power-law cooling tail. As $k \mapsto \infty$ the solutions resemble g_∞.

For other forms of g one must resort to numerical integration to follow their evolution. Thomas (1988b) looked at the steady-state evolution of a range of distributions with a sharp cut-off at low densities and reached the following conclusions:

- All distributions develop a high-density tail, $f \sim \rho^{-(4-\alpha)}$, as they cool.
- Sufficiently narrow distributions resemble the pure power-law g_1 by the time they begin to be deposited.

g_1 and g_∞ bound all reasonable solutions of the cooling flow equations, be they self-similar in form or not. In principle, k could be less than unity (as $k \mapsto 0$ the flow tends to the homogeneous case) but it is difficult to see how such distributions could arise. If the large density variations inferred within the cooling radius result from amplification of an initially much narrower distribution, then values of k of order unity are to be preferred. Without a plausible formation history for the ICM, however, it is better to leave k as a free parameter to be determined empirically. I will argue below that low values of k fit the observations of cooling flows in Abell clusters better than high values.

3 RECONSTRUCTION OF CLUSTER MASS PROFILES

The self-similar density distributions derived in Section 2 lead to particularly simple forms of the steady-state cooling flow equations. I derive these below and then show in the next section how they can be combined with the emissivity profile to provide strong constraints of the mass distribution within the cooling radius.

3.1 The equations

Substituting the functional form of g_k into equations A2, A3 and 3 we see that the self-similar forms of the cooling flow equations are:

$$\frac{\dot{\rho_0}}{\rho_0} - \frac{1}{\gamma}\frac{\dot{P}}{P} - \frac{\beta}{(2-\alpha)k} = 0 \tag{4}$$

and

$$\frac{\dot{\rho_0}}{\rho_0} + \nabla.\mathbf{u} + \beta = 0, \tag{5}$$

where

$$\beta = (2-\alpha)k\frac{\gamma-1}{\gamma}\frac{n_0^2\Lambda(T_0)}{P}. \tag{6}$$

To these may be added the equation of hydrostatic support,

$$\nabla\Phi + \frac{\nabla P}{\bar{\rho}} = 0, \tag{7}$$

where Φ is the gravitational potential. I assume here that the inflow is subsonic—this turns out to be a good approximation in all multiphase cooling flow models.

In a steady-state and spherical symmetry the above equations reduce to

$$\frac{\mathrm{d}\ln P}{\mathrm{d}\ln r} = -2\Sigma, \tag{8}$$

$$\frac{\mathrm{d}\ln \bar{\rho}}{\mathrm{d}\ln r} = -\frac{2}{\gamma}\Sigma - \frac{\tau}{2-\alpha}, \tag{9}$$

and

$$\frac{\mathrm{d}\ln u}{\mathrm{d}\ln r} = -2 + \frac{2}{\gamma}\Sigma + \left(\frac{1}{2-\alpha} + k\right)\tau, \tag{10}$$

where

$$\Sigma = \frac{GM}{2r}.\frac{\mu m_H}{k_B T} \tag{11}$$

is the ratio of the virial to the thermal temperatures, and

$$\tau = (2-\alpha)\frac{\gamma-1}{\gamma}\frac{n_0^2\Lambda(T_0)}{P}\frac{r}{u} = \frac{1}{k}\frac{\mathrm{d}\ln \dot{M}}{\mathrm{d}\ln r} \tag{12}$$

is the ratio of the inflow time to the constant-pressure cooling time.

Although there appear to be three equations here, the dimensionless ratios Σ and τ are the only important variables. The third equation merely acts as a scaling (for fixed τ, $\bar{\rho}^{2-\alpha} \propto p^{1-\alpha}u$). Hence the physics can be captured in just two equations:

$$\frac{\mathrm{d}\ln \Sigma}{\mathrm{d}\ln r} = \chi - 1 + 2\frac{\gamma-1}{\gamma}\Sigma - \frac{\tau}{2-\alpha} \tag{13}$$

and

$$\frac{\mathrm{d}\ln \tau}{\mathrm{d}\ln r} = 3 - \frac{2}{\gamma}\big[(3-\alpha) - \gamma(1-\alpha)\big]\Sigma - \left(\frac{3-\alpha}{2-\alpha} + k\right)\tau \tag{14}$$

where $\chi \equiv \mathrm{d}\ln M/\mathrm{d}\ln r$. The g_∞ equations can be recovered by letting $k \mapsto \infty$ and using $k\tau$ in place of τ as the second dimensionless variable.

The usual way of proceeding when solving the single-phase equations is to pick a functional form for the mass profile, χ, and mass deposition rate, β, then to solve for Σ and τ. From this one can generate an emissivity profile, $\xi(r)$, for comparison with the data. Here I adopt a different approach: because β is fixed (for a particular value of k) in the multiphase models, one can specify $\xi(r)$ and *determine* the mass profile.

Suppose that $\beta_{\rm fit} \equiv -(1/6)\mathrm{d}\ln\xi/\mathrm{d}\ln r$ is known. Then

$$\frac{\mathrm{d}\ln \tau}{\mathrm{d}\ln r} = 3 \quad - \quad 6\frac{(3-\alpha)-\gamma(1-\alpha)}{2-\alpha+\alpha\gamma}\beta_{\rm fit} \quad - \quad \left(\frac{2\gamma}{(2-\alpha)(2-\alpha+\alpha\gamma)} + k\right)\tau. \tag{15}$$

Furthermore this is an eigenvalue problem: requiring that the solution extend to $r = 0$ fixes the outer boundary condition. Hence we can solve for τ, Σ and χ.

3.2 The behaviour of solutions

We can get a good idea of the behaviour of the solutions to equation 15 by looking at the case of constant $\beta_{\rm fit}$. Imposing the physical constraints $\Sigma \geq 0$ (i.e. a non-negative

temperature) and $\chi \geq 0$ (i.e. mass constant or increasing with radius) restricts $\beta_{\rm fit}$ to lie in the range

$$\frac{3}{2(5+3\,k)} \leq \beta_{\rm fit} \leq \frac{80+21\,k}{120+36\,k} \tag{16}$$

(in this expression and henceforth I set $\gamma = 5/3$ and $\alpha = 0.5$ rather than including them explicitly). Thus steep emissivity profiles, $\beta_{\rm fit} \gtrsim 0.65$, are incompatible will all steady-state cooling flow models (larger values can occur, however, outside the cooling radius). In addition, the inner value of $\beta_{\rm fit}$ can be used to constrain k: flat cores are inconsistent with small values of k and a central decrease in emissivity would be incompatible with all models. If we assume that the virial temperature drops (i.e. $\Sigma \mapsto 0$) within the cluster core, then the central value of $\beta_{\rm fit}$ provides a *measure* of k.

The numerical solutions of equation 15 in the case of non-constant $\beta_{\rm fit}$ are illustrated in Figure 1. Here I have set $\beta_{\rm fit} = 0.6 + 0.1\,\log_{10} r$ and $k = 1$. Panel (a) shows the speed at which solutions diverge away from the desired one (i.e. the one which extends to $r = 0$) as r decreases. This ensures that the solutions are insensitive to the inner boundary condition and are stable to small variations in the value of $\beta_{\rm fit}$ in the inner bin (which is most likely to be affected by the point-spread function, uncertain absorption correction, etc.). The difference in the two values of τ at $r = 10^{-3}$ in the figure is less than one percent. Panel (b) shows that the solutions are able to cope with quite large variations in $\beta_{\rm fit}$: in this case 100 fluctuations drawn from a uniform distribution of extent ± 0.1 have been added to each decade in r. Despite the fact that $\beta_{\rm fit}$ now varies outside both ends of the physical range described in equation 16, it remains true to the smooth solution. In this paper we will fit smooth functions to observed emissivity profiles before attempting to solve the cooling flow equations.

4 APPLICATION TO ABELL CLUSTERS

I will now apply the above theory to three cooling flow clusters: A 85, A 745 and A 2025. The ROSAT HRI data were kindly supplied to me by Clovis Peres in the form of deprojected density and temperature profiles. This has the advantage that conversion of the counts into emissivity, including correction for the spectral response and absorption, has already been included. Provided that the cooling flow solutions resemble the deprojected one, then these corrections will hold good.

I will consider each of the clusters in turn.

4.1 A 85

The emissivity profile is shown in Figure 2. There are 23 annular bins, each 12 arcsec wide, of which the inner 9 have cooling times less than 1.33×10^{10}yr (throughout this paper I take $H_0 = 50\,{\rm km\,s^{-1}Mpc^{-1}}$). The profile is well-fit by a simple broken power-law fit,

$$\xi \propto \left[\left(\frac{r}{0.12\,{\rm Mpc}} \right)^{1.18} + \left(\frac{r}{0.12\,{\rm Mpc}} \right)^{2.83} \right]^{-1} . \tag{17}$$

The asymptotic slope of ξ as $k \mapsto 0$ is very close to the minimum permitted for $k = 1$ which suggests that the solution

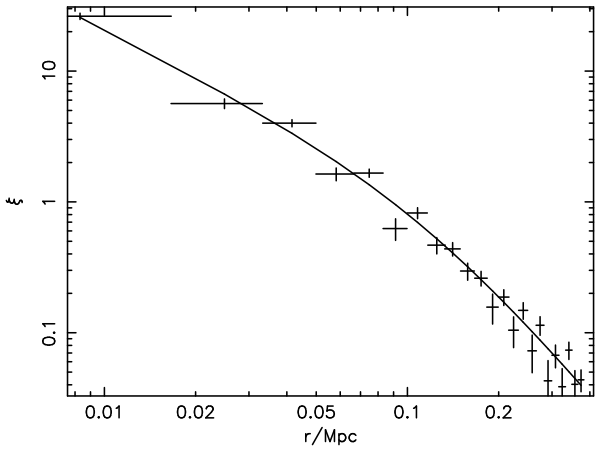

Figure 2. The emissivity profile for A85 in 12 arcsec bins. The solid line shows a broken power-law fit as described in the text.

will require an inner core in the mass distribution. This is illustrated in Figure 3. Note that Σ drops very close to zero at $r = 10\,{\rm kpc}$ (it tends to a small constant value within this radius). The gravitational density profile (i.e. that of the total mass, not just the gas) is well-fit at radii greater than 20 kpc by a King model,

$$\rho_{\rm grav} \propto \left[1 + \left(\frac{r}{0.11\,{\rm Mpc}} \right)^2 \right]^{-1.25} . \tag{18}$$

Within this radius the density is poorly constrained. Although it appears to rise, only a small change in the slope of ξ would cause it to level off or even fall—all we know for sure is that the virial temperature becomes very small. Note also that there is only one bin within 20 kpc and this one is most likely to be affected by smoothing by the point-spread function, uncertain correction for excess absorption, etc.

The temperature of the gas is approximately constant outside the core radius, but drops by a factor of five in to 10 kpc. A temperature decline in the centre of clusters is typical of cooling flows observed by ASCA.

Note that the slope of the mass-deposition profile, τ, is close to unity within the cooling radius, $r_{\rm cool} \approx 150\,{\rm kpc}$. This radius is not a special one for our solutions as we have assumed the cooling flow solution holds everywhere. For this reason the asymptotic slope of the gravitational density profile at larger radii should be taken with a pinch of salt.

The corresponding solution for $k = \infty$ is shown in Figure 4. There in no core in the gravitational mass profile in this case, with $\rho_{\rm dark}$ rising as r^{-2} all the way into 10 kpc. This is reflected in the temperature profile, however, which also rises by a factor of 5 between 150 and 10 kpc, unlike any observed cluster.

4.2 A 745

The emissivity profile, shown in Figure 5, has 19 bins of width 8 arcsec, with 9–12 bins interior to the cooling radius ($r_{\rm cool} \approx 180$–$240\,{\rm kpc}$). The first thing to note is that ξ flattens considerably in the innermost bin. This is incompatible

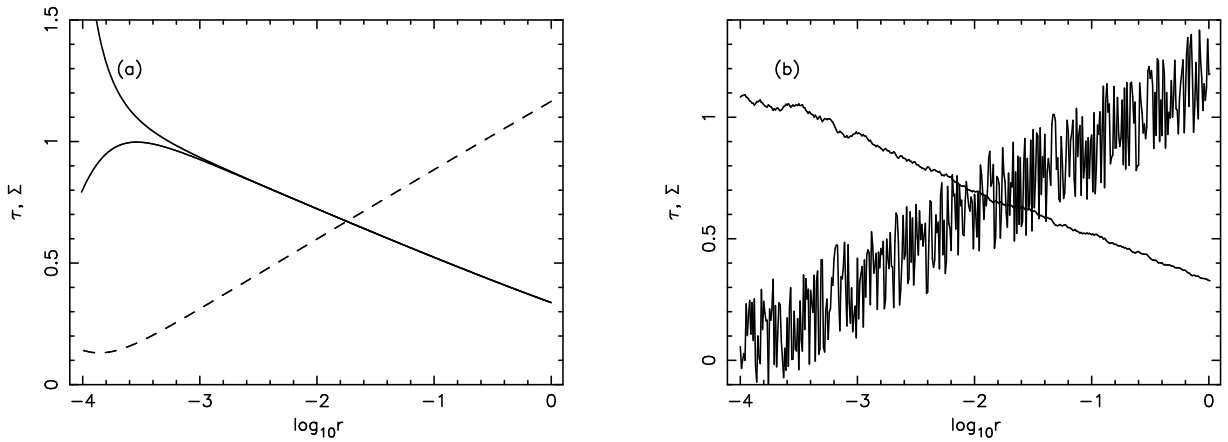

Figure 1. Solutions to the multiphase cooling flow equation, equation 15, for simple test profiles: (a) $\beta_{\rm fit} = 0.6 + 0.1 \log_{10} r$, (b) $\beta_{\rm fit} = 0.6 + 0.1 \log_{10} r \pm 0.1$. The curves which decline and increase with radius represent solutions for τ and Σ, respectively.

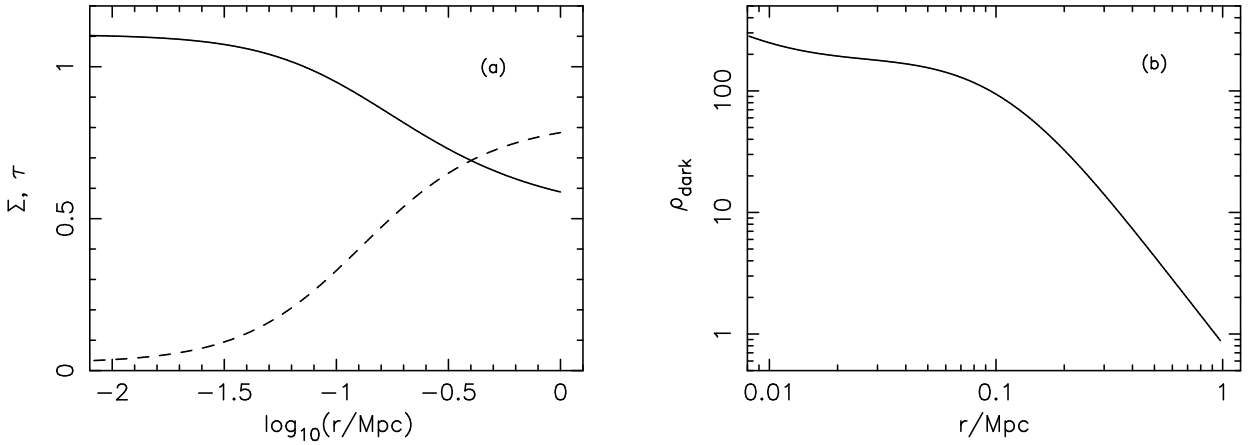

Figure 3. The $k = 1$ cooling flow solution for A85; (a) Σ (dashed line) and τ (solid line), (b) the density of the gravitating matter.

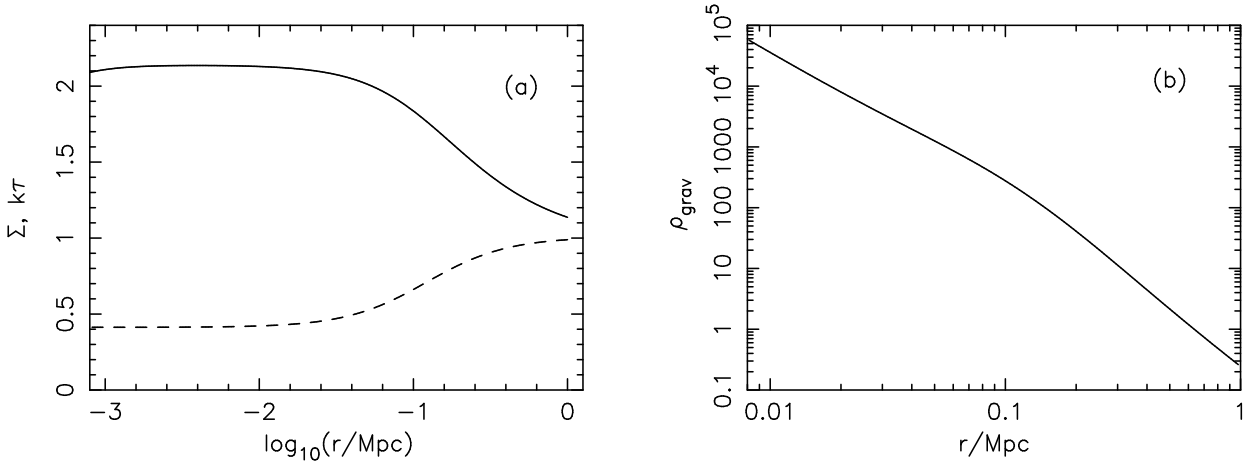

Figure 4. The $k = \infty$ cooling flow solution for A85; (a) Σ (dashed line) and τ (solid line), (b) the density of the gravitating matter.

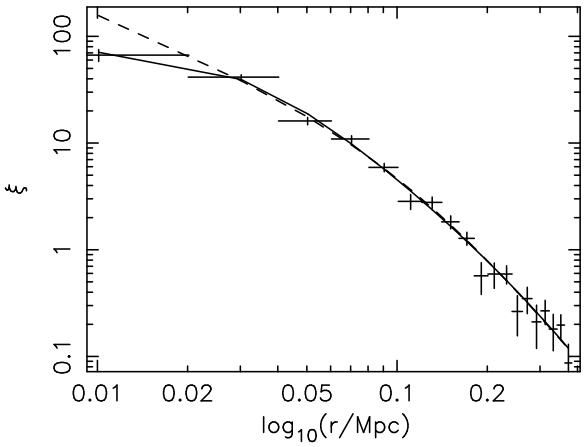

Figure 5. The emissivity profile for A745 in 8 arcsec bins. The solid line shows an analytic fit to the data and the dashed line shows the emissivity profile corresponding to a King-law density profile, as described in the text.

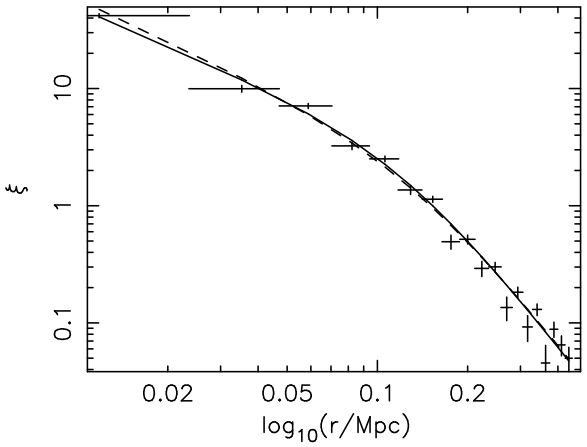

Figure 6. The emissivity profile for A2029 in 12 arcsec bins. The solid line shows an analytic fit to the data and the dashed line shows the emissivity profile corresponding to an analytic density profile, as described in the text.

with density distributions with small values of k. In fact the fit shown by the solid line,

$$\xi \propto \left[1 + \left(\frac{r}{31\,\mathrm{kpc}}\right)^{2.28} + \left(\frac{r}{89\,\mathrm{kpc}}\right)^{4.09}\right]^{-1} \tag{19}$$

admits solutions which extend to $r = 0$ only for $k = \infty$. Unfortunately, just as for A 85, large values of k give steeply rising dark-matter density and temperature profiles at small radii.

If we ignore the inner bin, however, then it is possible to find solutions for all values of k. The dotted line in Figure 5 shows the emissivity profile which corresponds to a mass density

$$\rho_{\mathrm{grav}} \propto \left[1 + \left(\frac{r}{0.11\,\mathrm{Mpc}}\right)^{2}\right]^{-1.57}. \tag{20}$$

and $k = 1$.

4.3 A 2029

For A 2029 there are 7–9 bins of width 12 arcsec within the cooling radius, $r_{\mathrm{cool}} approx 170$–$210\,\mathrm{kpc}$. The emissivity profile

$$\xi \propto \left[\left(\frac{r}{0.13\,\mathrm{Mpc}}\right)^{1.09} + \left(\frac{r}{0.13\,\mathrm{Mpc}}\right)^{3.34}\right]^{-1}. \tag{21}$$

shown in Figure 6 is again too shallow in the central bin, but the inconsistency is this time so slight that it strengthens the case for $k = 1$ (as discussed in Section 3.2 the slope of the emissivity profile within the cluster core provides a measure of k). Figure 7a shows that Σ drops to a value close to zero within 30 kpc. This indicates that the virial temperature has sunk well below the gas temperature (i.e. the flow is isobaric within this radius). This is reflected in Figure 7b which shows the corresponding density profile. The latter is well-fit at radii greater than 80 kpc by a mass-density

$$\rho_{\mathrm{grav}} \propto \left[1 + \left(\frac{r}{0.14\,\mathrm{Mpc}}\right)^{3}\right]^{-1} \tag{22}$$

but declines rapidly within this radius. Only a small change in the emissivity profile is required to generate solutions in which the gravitational mass has a constant core density, as indicated by the dotted line in Figure 6 which reproduces the above density profile exactly.

5 CONCLUSIONS AND DISCUSSION

- I have rederived the cooling flow equations for self-similar density distributions. Two of these in particular are expected to bound the behaviour of all possible flows.
- The steady-state cooling flow equations are *not* compatible will all conceivable emissivity profiles. Thus they can be used as a test of the theory.
- The solutions provide bounds on $M(r)$ within the cooling radius and given k can be used to measure $M(r)$.
- ROSAT HRI surface brightness data from three Abell clusters are best-fit by models in which $k \approx 1$. The measured core radii are then 110–140 h_{50}^{-1} kpc. Larger values of k give smaller (or non-existent) core radii, but have gas temperatures which rise sharply at small radii, in contrast with the observations.

It is unfortunate that the core radii deduced for the matter distributions for the Abell clusters under investigation are only slightly smaller than the radii of the cooling flows. It is possible that the self-similar, steady-state assumption is a poor one at the edge of the flow (it is also possible that it is valid well beyond the cooling radius) and that models could be found which were consistent with a much larger core radius.

Ideally, one would like a much better resolution at smaller radii, so that the tendency of the emissivity profile to a constant slope, indicative of the particular value of k, could be checked. This should be possible for some of the closer clusters, such as Virgo.

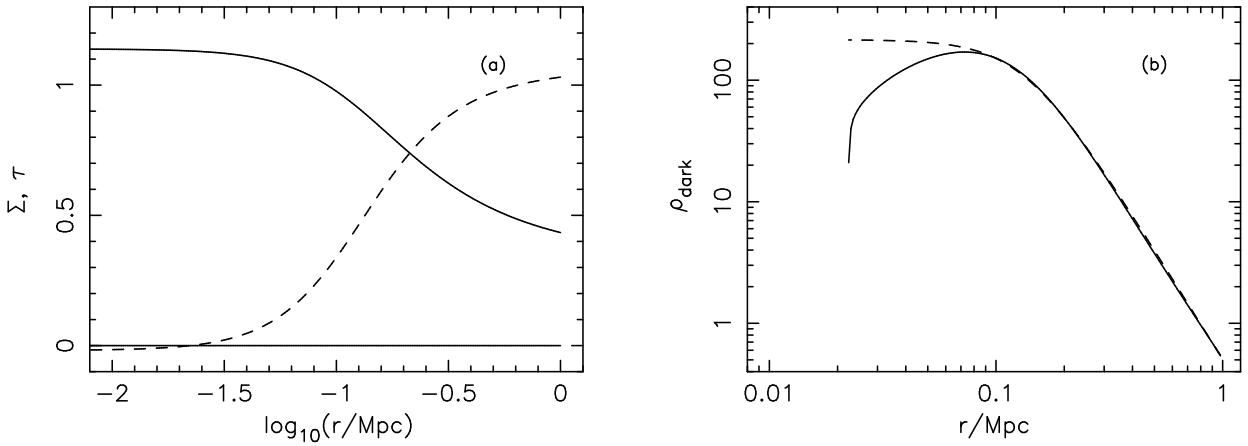

Figure 7. The $k = 1$ cooling flow solution for A2029; (a) Σ (dashed line) and τ (solid line), (b) the density of the gravitating matter (solid line) and an analytic fit as described in the text (dashed line).

Note that the solutions for Σ and τ given in this paper do not depend upon the normalisations of the gas and total gravitational masses. If desired, these can be determined by fixing the overall temperature and luminosity. The analysis of Gunn & Thomas (1996) shows that the gas density will be slightly lower and the total mass density slightly higher than in the equivalent single-phase analysis.

Cooling flows in individual galaxies are much better resolved than those in clusters and so look like promising candidates for the kind of modelling discussed here. However, the lower temperatures leads to complications such as a varying slope, α, for the cooling function, and larger corrections for absorption and emission lying outside the passband of the detector. There may also be sources of mass and energy injection into the flow.

ACKNOWLEDGMENTS

This paper was prepared using the facilities of the STARLINK minor node at Sussex. It was written while PAT was holding a Nuffield Foundation Science Research Fellowship.

REFERENCES

Gunn K. F., Thomas P. A., 1996, MNRAS, 281, 1133
Nulsen P. E. J., 1986, MNRAS, 221, 377
Thomas P. A., 1988a, in Fabian A. C., ed, NATO ASI Cooling flows in clusters and galaxies. Kluwer, Dordrecht, p. 361
Thomas P. A., 1988b, MNRAS, 235, 315
Thomas P. A., Fabian A. C., Nulsen P. E. J. N., 1987, MNRAS, 228, 973

APPENDIX A: DERIVATION OF THE MULTIPHASE COOLING FLOW EQUATIONS

We assume an emulsion of density phases which comove with the flow. The distribution is described by the volume fraction, $f(\rho, \mathbf{r}, t)$, such that $f\,\mathrm{d}\rho$ is the fractional volume occupied by phases with densities in the range ρ to $\rho + \mathrm{d}\rho$. Then $\int f\,\mathrm{d}\rho = 1$, and the mean density is $\bar{\rho} = \int f\rho\,\mathrm{d}\rho$.

Mass conservation gives

$$\frac{\partial}{\partial t}(\rho f) + \nabla.(\mathbf{u}\rho f) + \frac{\partial}{\partial \rho}(\dot{\rho}\rho f) = 0, \tag{A1}$$

where $\mathbf{u}$ is the rate of change of position and $\dot{\rho}$ is the rate of change of density following the flow. The final term in equation A1 is the equivalent in density space of the divergence in velocity space.

Integrating over all densities we obtain

$$\frac{\dot{\bar{\rho}}}{\bar{\rho}} + \nabla.\mathbf{u} + \beta = 0, \tag{A2}$$

where

$$\beta \equiv \frac{1}{\bar{\rho}} \lim_{\rho \mapsto \infty} (\dot{\rho}\rho f). \tag{A3}$$

This is equivalent to the usual single-phase equation (e.g. Thomas 1988a) except that the mass deposition rate is specified in terms of f rather than being a free parameter.

To find how the volume fraction changes with time we use the energy equation,

$$\rho\dot{s} = -n^2\Lambda, \tag{A4}$$

where s is the entropy and $n^2\Lambda$ is the radiated power per unit volume. For a fully-ionised plasma

$$s \equiv \frac{1}{\gamma - 1}\frac{k_B}{\mu m_H} \ln\left(\frac{P}{\rho^\gamma}\right). \tag{A5}$$

where P is the pressure, k_B is the Boltzmann constant, μm_H is the mass per particle and $\gamma = 5/3$. Then

$$\frac{\dot{\rho}}{\rho} = \frac{1}{\gamma}\frac{\dot{P}}{P} + \frac{\gamma - 1}{\gamma}\frac{n^2\Lambda}{P}. \tag{A6}$$

Over a wide temperature range appropriate to clusters the cooling function can be approximated by a power-law, $\Lambda \propto T^\alpha$, where $\alpha \approx 0.5$. Then equation A6 can be simplified by moving to a new density variable. Writing

$$\rho = \rho_0(\mathbf{r}, t) w^{-1/(2-\alpha)}, \tag{A7}$$

we obtain

$$\dot{w} = (2-\alpha)\left(\frac{\dot{\rho_0}}{\rho_0} - \frac{1}{\gamma}\frac{\dot{P}}{P}\right) w - (2-\alpha)\frac{\gamma-1}{\gamma}\frac{n_0^2\Lambda(T_0)}{P}. \quad \text{(A8)}$$

If the adiabatic compression term is removed by setting $P \propto \rho_0^\gamma$, then the energy equation takes a particularly simple form, $\dot{w}$ =constant. However, a more useful choice is to take $\rho_0 \propto \bar{\rho}$. From the final term of equation A1, we see that at high density when cooling is dominant, then $\dot{\rho}\rho f \sim$constant. This motivates the substitution

$$f = \frac{(2-\alpha)}{\rho_0} w^{(4-\alpha)/(2-\alpha)} g(w, \mathbf{r}, t). \quad \text{(A9)}$$

Then, using equations A1, A6 and A8 we obtain the following equation for the covariant derivate of g (i.e. following the fluid flow):

$$\frac{\dot{g}}{g} + (3-\alpha)\frac{\dot{\rho_0}}{\rho_0} - \frac{2-\alpha}{\gamma}\frac{\dot{P}}{P} + \nabla.\mathbf{u} = 0. \quad \text{(A10)}$$